Real-Time Differential Carrier Phase GPS-Aided INS

Jay A. Farrell, *Senior Member, IEEE*, Tony D. Givargis, and Matthew J. Barth, *Member, IEEE*

***Abstract*—This article describes the implementation and experimental results of a real-time carrier phase differential global positioning system (GPS) aided inertial navigation system (INS). The implementation is the result of a study to analyze the capabilities of such a system relative to the requirements of advanced vehicle control and safety systems (AVCSS) for intelligent transportation systems. Such navigation systems have many application possibilities (e.g., aviation and precision flight, automated mining, precision farming, dredging, satellite attitude control). Advantages and disadvantages of the GPS, INS, and differential GPS-aided INS approaches are discussed. The implementation achieves 100-Hz vehicle state estimates with position accuracies at the centimeter level through the use of differential carrier phase GPS techniques.**

***Index Terms*—Global positioning system, inertial navigation, Kalman filters, motion measurement, navigation, position control.**

I. Introduction

AUTOMATED vehicle position control systems require both a means for determining vehicle position and a means for controlling the vehicle position [11], [20]. This article focuses on an integrated carrier phase differential global positioning system/inertial navigation system (GPS/INS) approach to vehicle position (and state) determination.

The system specifications are based predominantly on advanced vehicle control and safety system (AVCSS) needs. Previous successful vehicle control experience [14], [22] demonstrated that a sample rate of at least 25 Hz and centimeter level position accuracy are sufficient for vehicle control under nominal operating conditions. Due to chassis and actuator dynamics, the control system bandwidth is less than 2 Hz under nominal driving conditions. Therefore, a navigation bandwidth of 10 Hz was deemed sufficient, but higher bandwidth is preferred to support the possibility of emergency maneuvering. Navigation systems achieving these specifications also have application possibilities in automated mining and dredging, aviation and precision flight, precision farming, and satellite attitude control.

This article describes the implementation and experimental results of a GPS-aided INS system designed to exceed these accuracy, bandwidth, and update rate specifications. Numerous previous applications have implemented pseudo-range-based GPS-aided INS systems (e.g., [17], [19]). The main novel feature of this application is the integration of INS and differential *carrier phase* GPS in real-time to achieve the centimeter level positioning requirement. Standalone carrier phase GPS positioning has been demonstrated to achieve centimeter level accuracy [1], [4], [5], [15], but to the authors' knowledge, this is the first paper describing an implementation and experiments that successfully demonstrate a real-time, differential carrier phase GPS-aided INS achieving centimeter accuracy.

Manuscript received November 16, 1998. Recommended by Associate Editor, K. Hunt.

J. Farrell and M. Barth are with the Department of Electrical Engineering, College of Engineering at the University of California, Riverside, CA 92521 USA.

T. Givargis is with the Department of Computer Science and Engineering, College of Engineering at the University of California, Riverside, CA 92521 USA.

Publisher Item Identifier S 1063-6536(00)05748-1.

II. Background

The following subsections review the advantages and disadvantages of GPS and INS technologies and motivate an integrated approach.

A. Global Positioning System and Vehicle Control

The accuracy of standard GPS position estimates is on the order of 100 m (R95[1]). Increased accuracy (at the meter level) can be achieved through the use of differential GPS (DGPS) (see, e.g., [1], [9], [10], [18]). Furthermore, a DGPS system that uses carrier phase observations can provide position accuracies of 1 to 3 cm [1], [4], [5], [15].

For vehicle control, a trajectory corresponding to the desired path could be defined in the global coordinate reference frame and stored on-board the vehicle. If desired, additional information such as the surface inclination, turning radius and direction, and super-elevation angle could also be stored on-board (e.g., using CD technology) as a function of path position to improve control performance. The vehicle control system would then drive the steering and propulsion actuation systems to force the vehicle to follow the desired trajectory.

Advantages of performing control in a global coordinate system are: 1) both lateral and longitudinal position information relative to the desired trajectory are known at all times; 2) the vehicle can always return to the desired path since it always knows its position and the desired position; 3) significant amounts of path preview information can be used to facilitate control [14]; 4) the vehicle velocity profile as a function of global position can be specified; and 5) the global position of the vehicle is available for other purposes (e.g., traveler information, traffic management, data logging). Additional advantages of using GPS include: 1) no changes are required to the environment (i.e., special markers, radar reflective paint, etc. are not required); 2) advanced GPS techniques could determine three-dimensional vehicle attitude; and 3) GPS signals are available in all weather conditions. The main drawbacks of a navigation system based solely on the GPS are 1) the satellite signals can be blocked by obstacles; 2) the GPS outputs are at a relatively low rate ($\leq$ 20 Hz); and 3) the GPS receiver outputs typically have a significant latency. Although the second and third items may be addressed through

[1]Size of the circle with 95% probability of containing the correct position.

improvements in receiver technology, the first disadvantage can only be overcome via integration of alternative technologies (e.g., INS or pseudolites).

B. Inertial Navigation and Vehicle Control

For control purposes, it is desirable to know the vehicle state[2] and inertial information (i.e., angular rates and linear acceleration) at high ($\geq$ 50 Hz) sampling rates. For reliable control operation, this information must be reliably available (i.e., no missing samples) at each sampling instant (i.e., with minimal latency).

INS [2], [6], [9] can provide the vehicle state information at rates suitable for accurate vehicle control. A typical INS system integrates the differential equation describing the system kinematics for a short period of time using high rate data from inertial instruments. During this integration process, the error variance of the navigation state increases due to sensor noise and inaccuracies in sensor calibration and alignment. After a period of integration, aiding sensor measurements (e.g., GPS) can be used to correct the state estimates. The main advantages of INS systems are: 1) vehicle state estimates are produced without differentiation (i.e., low sensitivity to high-frequency noise); and 2) the accuracy of the INS state is not affected by fields external to the INS. The main disadvantage of an unaided INS system is unbounded growth in the position estimation error; however, an INS system used in conjunction with aiding sensors can provide the state estimate at the desired control frequency more accurately than either technique used independently. Additional advantages of an aided INS system are: 1) the update rate of the navigation state estimates is not limited by the update rates of the aiding sensors; and 2) the INS estimate of the vehicle state is available at the desired sampling instants regardless of the latencies in the aiding sensors. In addition, the INS continues to provide position estimates at times when signals from the aiding system were not available. During such periods, the INS accuracy can be accurately predicted. This accuracy can be used in higher level reasoning loops to maintain or switch modes of operation.

C. Summary: Redundant Positioning Systems

As the previous sections have described, INS and GPS have complementary characteristics. When GPS information is available, a GPS-aided INS can provide accurate high-rate high-bandwidth vehicle state information. The GPS aiding information is used to estimate errors in the INS state and to calibrate the inertial sensors. This results in improved INS accuracy. During periods when signals from some or all of the GPS satellites become unavailable, the INS continues to provide vehicle state information. Therefore, the integrated approach results in reliability, latency, bandwidth, and update rate improvements relative to the GPS only approach. to correct the INS state).

The objective of this project was to design and implement a GPS-aided INS satisfying the accuracy and update rate specifications required for the AVCSS application. Based on such demonstrations, GPS-aided INS techniques can be seriously considered along with other referencing systems if three viable independent systems are to be available for AVCSS. Although AVCSS was the primary motivation for this GPS-aided INS development project, many other applications are possible.

[2]Within this article the term "vehicle state" will be used to refer to the following set of vehicle information: three-dimensional position, three-dimensional velocity, and three-dimensional attitude.

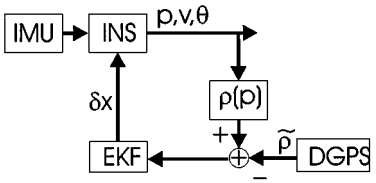

Fig. 1. Complementary filter.

III. Methodology

The navigation system developed for this project incorporates a strapdown INS with various modes of GPS aiding. The following sections discuss each component of the system design. Section III-A describes the overall approach. Section III-B discusses the INS implementation and error equations. Section III-C discusses various issues related to obtaining high accuracy position information from the GPS. Section III-D discusses the method used to resolve carrier phase integer ambiguities. Section IV presents the algorithms used to calculate the continuous-time equivalent discrete-time state transition and process noise covariance matrices. Section V discusses various specific issues related to the system design.

A. GPS-Aided INS

Fig. 1 shows a block diagram of the GPS-aided INS implemented for this project. This implementation is referred to as a complementary filter [3]. The noisy inertial measurement unit (IMU) outputs are processed by the INS. Since the INS is an integrative process, the output of the INS is the actual state plus a predominantly low-frequency error. The INS output is processed to provide an estimate of the GPS measurement. The difference between the estimated GPS output and the measured differential GPS output is a signal that contains two noise components—the predominantly low-frequency INS component and the predominantly high-frequency differential GPS component. The frequency content of each noise component can be accurately modeled. The objective of the state estimation design is to attenuate the GPS measurement error and provide an accurate estimate of the INS state error denoted in the following by $\delta\mathbf{x}$. Therefore, the state estimator has a predominantly low-pass characteristic. Subtracting the error estimate from the INS state, in a well-designed system, produces an accurate estimate of the navigation state. As shown in Fig. 1, the complementary filter was implemented in feedback form (i.e., the estimated position, velocity, Euler angles, and instrument errors were fed back

In the complementary filter approach, the INS is the primary navigation system which calculates the navigation state at the high rate at which it is used for control, guidance, and planning functions. The DGPS aiding information is used when it is available and satisfies conditions designed to verify proper sensor operation. When such aiding sensor information is not available or judged inaccurate, the INS continues its normal (unaided) operation (i.e., transformation and integration of the IMU outputs).

During either aided or unaided operation, the error covariance matrices propagated within the state estimation approach predict the accuracy of the state estimates (for use in higher level reasoning loops).

The INS provides a reference trajectory around which the system equations are linearized. The error state estimator is implemented by an extended Kalman filter (EKF) using the linearized error dynamics presented in Section III-B and the linearized observation matrix. All driving noise spectral densities were estimated from experimental data.

The main advantages of the complementary filter approach are that 1) the high rate INS state is available without latency regardless of the availability and latency of the GPS aiding information; (2) the EKF inputs can be accurately modeled as stochastic processes, as appropriate for the technique [3]; and, (3) the computationally intensive error covariance propagation equations can be implemented at a low update rate even though the navigation state is calculated at the desired rate of the control system.

The following sections focus on material necessary to specify our approach. To meet the page limitations, equations that are available in the literature in an appropriate form are specified by citation. Derivations using the same notation can be found in [9]. Computed and measured variables are denoted, respectively, by $\hat{x}$ and $\tilde{x}$.

B. Tangent Plane Implementation

The (local fixed) tangent plane INS differential equations are defined by [9, eq. (6.44), (6.51), and (6.52)]. The navigation state is $\mathbf{x} = [\mathbf{p}, \mathbf{v}, \boldsymbol{\rho}]$ where $\mathbf{p} = (n, e, d)$ is the position vector, $\mathbf{v} = (v_n, v_e, v_u)$ is the tangent plane velocity, and $\boldsymbol{\rho} = [\phi, \theta, \psi]$ are the Euler angles. The local, fixed tangent plane INS was sufficient for this demonstration due to the limit geographic area expected for testing. Minor changes to the INS would be required if it was desired to transform the currently implemented INS to a geodetic (latitude, longitude based) implementation. The INS mechanization equations are updated at 100 Hz, using the predictor–corrector integration routine.

For error analysis and error estimation via Kalman filtering, it is convenient to linearize the INS equations about the vehicle trajectory. The linearized error equations are derived in [9] and summarized below. The summary uses the notation $\omega_N = \omega_{ie}\cos(\lambda)$ and $\omega_D = -\omega_{ie}\sin(\lambda)$ for the north and vertical components of earth rotation rate in the navigation frame.

The linearized INS error dynamic equations are

$$\delta\dot{\mathbf{x}}(t) = \begin{bmatrix} \mathbf{F_{pp}} & \mathbf{F_{pv}} & \mathbf{F_{p\rho}} \\ \mathbf{F_{vp}} & \mathbf{F_{vv}} & \mathbf{F_{v\rho}} \\ \mathbf{F_{\rho p}} & \mathbf{F_{\rho v}} & \mathbf{F_{\rho\rho}} \end{bmatrix} \begin{bmatrix} \delta\mathbf{p} \\ \delta\mathbf{v} \\ \delta\boldsymbol{\rho} \end{bmatrix} + \begin{bmatrix} \mathbf{0} \\ \mathbf{e_v} + \omega_{\mathbf{v}} \\ \mathbf{e_\rho} + \omega_{\boldsymbol{\rho}} \end{bmatrix} \quad (1)$$

where the nominal error state is defined by $\delta\mathbf{p} = [\delta n, \delta e, \delta h]^T$, $\delta\mathbf{v}^n = [\delta v_N, \delta v_E, \delta v_D]^T$, and $\delta\boldsymbol{\rho}^n = [\delta\epsilon_N, \delta\epsilon_E, \delta\epsilon_D]^T$. The subcomponents of the $\mathbf{F}$ matrix are approximated as $\mathbf{F_{pp}} = \mathbf{F_{p\rho}} = \mathbf{F_{\rho p}} = \mathbf{F_{\rho v}} = \mathbf{F_{\rho\rho}} = \mathbf{0}$, $\mathbf{F_{pv}} = \text{diag}([1, 1, -1])$, $\mathbf{F_{vp}} = \text{diag}([0, 0, (-2\mu/R^3)])$, $\mathbf{F_{vv}} = 2([\omega_N, 0, \omega_D]\times)$, and $\mathbf{F_{v\rho}} = ([f_N, f_E, f_D]\times)$ where the notation $(\mathbf{v}\times)$ is defined in [9, Appendix A]. All error quantities are defined as the actual value minus the calculated quantity (i.e., $\delta x = x - \hat{x}$).

The velocity error is driven by accelerometer and gravitational model errors denoted by $\mathbf{e_v}$ in (1). The attitude error is driven by gyro errors denoted by $\mathbf{e_\rho}$ in (1). The state augmentation process [9], [13] is used to model the instrumentation and gravity errors as Markov process. The estimated state of such Markov processes is used to calibrate the instruments. Let $\mathbf{x}_a$ denote the state augmented to account for the accelerometer and gravitation errors. Let $\mathbf{x}_g$ denote the state augmented to account for the gyro errors. Suitable linearized error models are derived in, for example, [2], [9], [13]. The state augmentation process leads to a high-dimensional augmented error state, which for observability reasons was reduced to 15 states: the nine error states of (1), three accelerometer error states, and three gyro error states. In addition, two GPS clock bias states were appended to the error model, for a total of 17 error states.

The reduction of the high dimensioned error model to a reasonably sized model for on-line implementation was a time consuming process based on covariance studies and system simulation. Care was exercised to ensure that the error states that were neglected in the implementation model did not have a debilitating effect on the ultimate system performance. Due to the benign (i.e., low acceleration and angular rate) environment expected in the class of applications under consideration, this 17 state error model was predicted to be sufficient and ultimately did achieve the desired performance.

The resulting navigation system error model used in the on-line implementation is

$$\begin{bmatrix} \delta\dot{\mathbf{p}} \\ \delta\dot{\mathbf{v}} \\ \delta\dot{\boldsymbol{\rho}} \\ \dot{\mathbf{x}}_a \\ \dot{\mathbf{x}}_g \end{bmatrix} = \begin{bmatrix} \boldsymbol{\omega}_{\mathbf{p}} \\ \boldsymbol{\omega}_{\mathbf{v}} + \boldsymbol{\nu}_a \\ \boldsymbol{\omega}_{\boldsymbol{\rho}} + \boldsymbol{\nu}_g \\ \boldsymbol{\omega}_{\mathbf{a}} \\ \boldsymbol{\omega}_{\mathbf{g}} \end{bmatrix} + \begin{bmatrix} \mathbf{0} & \mathbf{F_{pv}} & \mathbf{0} & \mathbf{0} & \mathbf{0} \\ \mathbf{F_{vp}} & \mathbf{F_{vv}} & \mathbf{F_{v\rho}} & \mathbf{R}_{v2t} & \mathbf{0} \\ \mathbf{0} & \mathbf{0} & \mathbf{F_{\rho\rho}} & \mathbf{0} & \mathbf{R}_{v2t} \\ \mathbf{0} & \mathbf{0} & \mathbf{0} & \mathbf{F_{x_a x_a}} & \mathbf{0} \\ \mathbf{0} & \mathbf{0} & \mathbf{0} & \mathbf{0} & \mathbf{F_{x_g x_g}} \end{bmatrix} \begin{bmatrix} \delta\mathbf{p} \\ \delta\mathbf{v} \\ \delta\boldsymbol{\rho} \\ \mathbf{x}_a \\ \mathbf{x}_g \end{bmatrix}. \quad (2)$$

In this document, $\mathbf{x}_a$ and $\mathbf{x}_g$ are referred to as accelerometer and gyro biases, respectively. In actuality, they represent a composite of accelerometer and gyro errors. Modeling these states as random walk processes, $\mathbf{F_{x_a x_a}}$ and $\mathbf{F_{x_g x_g}}$ are identically zero. The power spectral densities for the driving noise processes $\boldsymbol{\omega}_{\mathbf{a}}$ and $\boldsymbol{\omega}_{\mathbf{g}}$ were determined by analysis of the instrument biases over an extended period of time. Similarly, the spectral density of the measurement noise processes $\boldsymbol{\nu}_a$ and $\boldsymbol{\nu}_g$ were determined by the analysis of measurement data.

C. GPS Processing

The following sections describe the processing necessary to use GPS measurements for INS aiding. Particular attention is focused on the processing necessary to use carrier phase information.

1) GPS Observables: The two basic outputs of a GPS receiver are pseudo-range and carrier phase (from [9])

$$\begin{aligned}\tilde{\rho}_1^{(i)} &= ((X^{(i)}-x)^2+(Y^{(i)}-y)^2+(Z^{(i)}-z)^2)^{0.5} \\ &\quad + c\Delta t_r + c\Delta t_{sv}^{(i)} + \frac{f_2}{f_1} I_a^{(i)} + SA^{(i)} + E^{(i)} \\ &\quad + MP^{(i)} + \eta^{(i)} \qquad (3) \\ \tilde{\phi}_1^{(i)} &= \Big[((X^{(i)}-x)^2+(Y^{(i)}-y)^2+(Z^{(i)}-z)^2)^{0.5} \\ &\quad + c\Delta t_r + c\Delta t_{sv}^{(i)} - \frac{f_2}{f_1} I_a^{(i)} + SA^{(i)} + E^{(i)} \\ &\quad + mp^{(i)} + \beta^{(i)}\Big] \frac{1}{\lambda_1} + N_1^{(i)} \qquad (4)\end{aligned}$$

where $\tilde{\rho}^{(i)}$ is the measured pseudorange to the ith satellite, $(X^{(i)}, Y^{(i)}, Z^{(i)})$ are the ECEF position coordinates of satellite i, (x, y, z) are the ECEF position coordinates of the receiver antenna, Δt_r is receiver clock bias, $\Delta t_{sv}^{(i)}$ is satellite clock bias, $I_a^{(i)}$ is atmospheric delay, $SA^{(i)}$ is the deliberate corruption of the satellite signals under the policy of selective availability, $E^{(i)}$ is error in the broadcast ephemeris data, $MP^{(i)}$ is multipath error on the civilian range signal, $mp^{(i)}$ is phase multipath error, $\eta^{(i)}$ is receiver range tracking error, $\beta^{(i)}$ is receiver phase tracking error, $\lambda_1 = (c/f_1)$ and c is the speed of light. The $()^{(i)}$ notation refers to the quantity in parenthesis to the ith satellite. A two frequency receiver will output range and phase measurements for each carrier frequency (L1: $f_1 = 1575.42$, L2: $f_2 = 1227.60$ MHz)

$$\begin{aligned}\tilde{\rho}_2^{(i)} &= ((X^{(i)}-x)^2+(Y^{(i)}-y)^2+(Z^{(i)}-z)^2)^{0.5} \\ &\quad + c\Delta t_r + c\Delta t_{sv}^{(i)} + \frac{f_1}{f_2} I_a^{(i)} + SA^{(i)} + E^{(i)} \\ &\quad + MP_2^{(i)} + \eta_2^{(i)} \qquad (5) \\ \tilde{\phi}_2^{(i)} &= \Big[((X^{(i)}-x)^2+(Y^{(i)}-y)^2+(Z^{(i)}-z)^2)^{0.5} \\ &\quad + c\Delta t_r + c\Delta t_{sv}^{(i)} - \frac{f_1}{f_2} I_a^{(i)} + SA^{(i)} + E^{(i)} \\ &\quad + mp_2^{(i)} + \beta_2^{(i)}\Big] \frac{1}{\lambda_2} + N_2^{(i)} \qquad (6)\end{aligned}$$

resulting in four basic outputs. In each of the four equations of this section, the first line of the equation represents the pseudo-range between the user and satellite antenna phase centers. It is referred to as a "pseudo" range since it is not a pure range signal. The GPS output prediction block of the complementary filter (i.e., $\rho(x)$ of Fig. 1) uses the first line of each of these four equations to predict the corresponding GPS pseudo-range measurements based on the INS position variables. The second line of each equation shows the manner in which each error source affects each measurement. The four right-most error sources in the second line of each equation are referred to as *common mode error sources*, as they are common to all receivers within a local operating area. Common mode error sources can be affectively removed by the differential GPS methods described in Section III-C.3.

Combinations of these four basic GPS outputs provide other (sometimes) useful signals. The basic outputs and their combinations are discussed in the following sections.

2) Measurement Matrix Definition: With the three position variables and the clock error, there are four unknown quantities in the standard GPS positioning application. The standard GPS positioning problem is to determine these four unknowns based on at least four pseudorange measurements.

To simplify the remaining discussion, let

$$\tilde{\rho}^{(i)}(\mathbf{x}) = \rho^{(i)}(\mathbf{x}) + \chi_1^{(i)}$$

where $\mathbf{x} = (x, y, z, c\Delta t_r)$, $\rho^{(i)}(\mathbf{x})$ are the terms involving $\mathbf{x}$ in the right-hand side of (3), and $\chi_1^{(i)}$ are the remaining terms in the right-hand side of (3). Linearization of a set of pseudo-range equations about the point $\mathbf{x}_0$ gives

$$\rho(\mathbf{x}) = \rho(\mathbf{x}_0) + \mathbf{H}(\mathbf{x}-\mathbf{x}_0) + \chi_1 + \text{h.o.t.'s} \qquad (7)$$

where h.o.t.'s represents the higher order terms in the expansion. The measurement matrix is defined using the notation of this article in [9, Sec. 5.3].

For implementation of the GPS-aided INS using a complementary filter (see Fig. 1), the INS will provide the point of linearization $\mathbf{x}_0$ at the time instant corresponding to the GPS measurements. Synchronization between the INS and GPS is possible since the GPS receiver supplies a one pulse per second signal that can be aligned with the GPS second. The measurement matrix $\mathbf{H}$, augmented with addition appropriately placed columns of zero vectors, will be used by the complementary filter to estimate the INS error state. Note that the position estimation accuracy will depend on both the numeric properties of $\mathbf{H}$ and the magnitude of χ_1.

In solving (7), the effective satellite vehicle (SV) positions and clock offsets are required. Both items can be computed using data derived from the GPS navigation messages as described in [9], [19].

3) Differential GPS Operation: The common mode error sources described previously severely limit the accuracy attainable using GPS. These errors are generally not observable using a single receiver unless its position is already known. However, the common mode errors are the same for all receivers in a local area. Therefore, if the errors could be estimated by one receiver and broadcast to all other receivers, the GPS accuracy could be substantially improved [19]. Three differential GPS (DGPS) techniques are described in [9]. Range based differential GPS was selected for this implementation as this approach allows the most flexibility in a system involving multiple roving vehicles. Range space techniques allow each roving receiver to choose the best set of satellites for its circumstance.

Differential GPS involves a GPS receiver/antenna at a known location (x_o, y_o, z_o), a receiver/antenna at an unknown possibly changing position (x, y, z), and a communication medium from the first receiver to the second receiver. The former receiver is referred to as the *base*, while the latter is referred to as the *rover*. One base station can service an unlimited number of rovers.

The common mode noise sources are continuous and slowly time varying and have significant short-term correlation [7],

[10]. Since the base station location is accurately known, it is straightforward for the base station to estimate the range and phase differential corrections for each of the carrier signals. The range correction for the L1 pseudo-range is a filtered version of

$$\Delta_{\mathrm{DGPS}}(t) = -\left(c\delta t_{sv}(t) + SA(t) + E(t) + \frac{f_2}{f_1} I_a\right). \quad (8)$$

Note that Δ_{DGPS} is compensated for base receiver and satellite clock bias (i.e., $\delta t_{sv} = \Delta t_{sv} - \hat{\Delta} t_{sv}$). Given that the corrections $\boldsymbol{\Delta}_{\mathrm{DGPS}}$ are available (by broadcast) at the rover for the satellites of interest, the DGPS position of each rover are calculated at the rover as

$$\hat{\mathbf{x}} = (\hat{\mathbf{H}}^T\hat{\mathbf{H}})^{-1}\hat{\mathbf{H}}^T(\tilde{\boldsymbol{\rho}} + \boldsymbol{\Delta}_{\mathrm{DGPS}}). \quad (9)$$

In a DGPS/INS implementation, the differentially corrected pseudo-range (i.e., $\tilde{\boldsymbol{\rho}} + \boldsymbol{\Delta}_{\mathrm{DGPS}}$) is used in place of the measured range in the EKF residual calculation equation.

Since the pseudo-range noncommon mode noise has a standard deviation between 0.1 and 4.0 m, depending on receiver design and multipath mitigation techniques, DGPS position accuracy is much better than standard GPS accuracy. Cancellation of the common mode noise sources in (9) assumes that the rover is sufficiently near (within 10–50 mi.) the base station and that the corrections are available at the rover in a timely fashion. For the implementation of this project, the base broadcast satellite identifiers, ephemeris set identifiers, reference time, and L1 and L2 phase and range corrections that were calculated by the method described in [7]. Latency compensation is discussed in [10]. Wide area DGPS techniques, served by a network of on the order of ten base stations, suitable for continent-wide DGPS service are discussed in [18].

4) Carrier Phase Observables: A receiver in phase lock on the carrier signal is able to track the relative phase shift in the carrier between any two time instants. Although the receiver cannot directly measure the number of carrier cycles between it and a given satellite, the receiver can accurately measure the change in this number of cycles. These facts result in an integer uncertainty in the number of cycles of the carrier between the satellite and user antenna at an initial measurement time. This integer is represented as N_1 in (4) and N_2 in (6). The integers N_1 and N_2 are referred to as *integer phase ambiguities*. Each integer ambiguity is a (usually large) unknown integer constant (barring loss of phase lock). To make use of the carrier phase observable as a range estimate, the integer ambiguity must be determined. If the integer ambiguity can be determined, then position determination based on phase measurements proceeds as described in the previous sections.

The interest in the carrier signal stems from the fact that the noncommon mode errors $mp^{(i)}$ and $\beta^{(i)}$ are much smaller than the respective errors on the code range observables. The common-mode errors are essentially the same as those on the code range observable, except that the ionospheric error enters (3) and (4) with opposite signs. Therefore, to take advantage of the small noncommon mode phase errors, the common mode phase errors must be removed. This is accomplished through differential operation.

In the differential mode of operation (see Section III-C.3), the common mode errors can be reduced to produce an observable accurate to a few centimeters. Let this differentially corrected phase be described as

$$\Delta\phi^{(i)}\lambda = \mathbf{h}^{(i)}(\mathbf{x} - \mathbf{x}_o) - (N^{(i)} - N_b^{(i)})\lambda \quad (10)$$

where the subscript in $(\zeta)_b^{(i)}$ refers the generic quantity ζ to the DGPS base station. The differentially corrected phase of (10) provides a very accurate measure of range assuming that the integer ambiguity has been determined. All phase measurements are corrupted by multipath and receiver noise. The corresponding error terms are dropped from the equations of this section for brevity, see [9].

Determination of the integer ambiguity for each satellite is the most critical issue that must be addressed prior to using the carrier phase measurement as an INS aiding signal. One approach is to augment one additional integer ambiguity "state" per satellite to the error model and to let the EKF estimate its value [16]. This approach has three disadvantages: 1) The integer nature of the integer ambiguity is lost, since the EKF estimates the additional state as a real variable; 2) The fact that the integer ambiguity is a constant is also lost, unless the range multipath is also modeled as an augmented state. If the range multipath is not modeled, then the single augmented state (per satellite) must represent both range multipath and integer ambiguity (see [9, Sec. 7.4]). This error state is neither integer nor constant. (3) The additional error states increases the computational burden of the EKF. Instead, the implementation described herein used an integer ambiguity search-based approach. The search technique is described in Section III-D. Section III-C5 defines an auxiliary phase variable referred to as the widelane phase [15] which, due to its larger wavelength, will be used to facilitate the integer search.

5) Wide and Narrow Lane Variables: The phase measurements of (10) at the L1 and L2 frequencies for a single satellite can be written as

$$(\tilde{\phi}_1 + N_1) = \frac{f_1}{c} r - \frac{f_2}{c} I_a \quad (11)$$

$$(\tilde{\phi}_2 + N_2) = \frac{f_2}{c} r - \frac{f_1}{c} I_a \quad (12)$$

where $\lambda_1 = (c/f_1)$ and $\lambda_2 = (c/f_2)$. The common mode errors have been eliminated through differential operation. The Δ's have been dropped for convenience of notation. For small differential distances, the residual ionospheric error I_a should be small. Define

$$\lambda_w = \frac{c}{f1 - f2} = 86.2 \text{ cm} \quad \text{and } \lambda_n = \frac{c}{f1 + f2} = 10.7 \text{ cm}.$$

Then, the difference of (11) and (12) results in the variable referred to as the wide lane phase measurement

$$(\tilde{\phi}_1 - \tilde{\phi}_2)\lambda_w = r + I_a - (N_1 - N_2)\lambda_w. \quad (13)$$

The pseudo-range measurements can be processed similarly yielding

$$\left(\frac{\tilde{\rho}_1}{\lambda_1}+\frac{\tilde{\rho}_2}{\lambda_2}\right)\lambda_n = r+I_a+\frac{\lambda_n}{\lambda_1}(MP_1+\eta_1)+\frac{\lambda_n}{\lambda_2}(MP_2+\eta_2).$$

Note that the right-hand sides of the above equations are directly comparable. Since the residual ionospheric delay and the carrier noise are expected to be small and the coefficient of the code noise is significantly less than one, the difference of the two equations, described as

$$\begin{aligned}&\left(\frac{\tilde{\rho}_1}{\lambda_1}+\frac{\tilde{\rho}_2}{\lambda_2}\right)\lambda_n-(\tilde{\phi}_1-\tilde{\phi}_2)\lambda_w\\&=(N_1-N_2)\lambda_w+\frac{\lambda_n}{\lambda_1}(MP_1+\eta_1)+\frac{\lambda_n}{\lambda_2}(MP_2+\eta_2)\end{aligned}\tag{14}$$

should provide a basis for estimating the wide lane integer (N_1-N_2). The standard deviation of the noise on each measurement of (N_1-N_2) produced by (14) is approximately 0.7 times the code multipath measured in meters. Therefore, the correct integer ambiguity can be reasonably expected to be within three integers of the estimate from (14). Averaging of the above estimate of (N_1-N_2) does not significantly decrease the estimation error unless the sampling time is long (i.e., minutes) since multipath is slowly time varying. Instead, an integer search will be required around the estimated value. Once this search is complete and (N_1-N_2) is determined, (13) is available for accurate carrier phase positioning and for aiding in direct estimation of the N_1 and N_2 variables.

D. Integer Ambiguity Resolution

The implemented integer search procedure is an extension of that described for GPS only positioning in [15], [23]. The method is extended to operate robustly using additional information that is available within an aided INS loop. An expanded description of the method in the context of recursive least squares estimation and hypothesis testing is presented in [9]. The method will be presented for a generic phase measurement and wavelength. In the implementation, the algorithm will be used to independently determine the widelane, L1, and L2 integers.

Consider a set of $n > 4$ differentially corrected residual (i.e., actual minus INS based prediction) phase measurements of wavelength λ

$$\begin{bmatrix}\tilde{\boldsymbol{\phi}}_p\\ \tilde{\boldsymbol{\phi}}_s\end{bmatrix}\lambda+\begin{bmatrix}\mathbf{N}_p\\ \mathbf{N}_s\end{bmatrix}\lambda=\begin{bmatrix}\mathbf{H}_p\\ \mathbf{H}_s\end{bmatrix}\mathbf{x}+\begin{bmatrix}\boldsymbol{\beta}_p\\ \boldsymbol{\beta}_s\end{bmatrix}\tag{15}$$

where the measurements are partitioned into a primary and a secondary measurement set. The ambiguity resolution algorithm proceeds by hypothesizing a set of integers for the primary set of measurements and using the secondary set of measurements as a test of each hypothesis. The primary set of measurements must have at least four satellites and these four should be selected to have a reasonable GDOP[3].

[3]Geometric dilution of precision. Good GDOP implies that the measurement matrix $\mathbf{H}$ is well conditioned [9], [19].

At the inception of the algorithm, $\tilde{\boldsymbol{\phi}}_p$, $\tilde{\boldsymbol{\phi}}_s$, $\mathbf{H}_p$, $\mathbf{H}_s$, and λ are known. The β terms are measurement noise, which will be neglected in the subsequent algorithm presentation. The objective is to determine the unknown vectors $\mathbf{N}_p$ and $\mathbf{N}_s$. The intermediate variable $\mathbf{x}=[\delta\mathbf{p}, c\delta t_r]$ represents the INS position error and rover receiver clock bias error. This variable will be estimated in the course of the algorithm. Since the complementary filter is implemented in feedback form, $\mathbf{x}$ should be small with a mean value of zero. The error covariance of this vector, which is propagated by the EKF, is available to the search algorithm.

Note that the solution to (15), as written, is not unique. Let the optimal values be denoted: $\mathbf{N}_p^*$, $\mathbf{N}_s^*$, $\delta\mathbf{p}^*$ and $c\delta t_r^*$. The vectors obtained by incrementing each element of $\mathbf{N}_p^*$ and $\mathbf{N}_s^*$ by i and incrementing $c\delta t_r^*$ by $i\lambda$ cannot be discriminated from the optimal values. To make the solution unique, the first integer is artificially set to zero. The clock bias that results from the algorithm is therefore $c\Delta t_r^*-N_1^*\lambda$. The remaining integers are also biased by N_1^* (i.e., $\mathbf{N}_p^*-N_1^*$ and $\mathbf{N}_s^*-N_1$ are actually found by the algorithm), where the integer N_1^* is not known. This issue will be addressed later.

1) Initialization of the Set of Candidate Integer Vectors: The search algorithm is implemented as a nested triple "for" loop. Prior to entering the loop, the following variables are defined to minimize calculations within the loop:

$$\mathbf{x}_{\boldsymbol{\phi}}=\mathbf{H}_p^{-1}\tilde{\boldsymbol{\phi}}_p\lambda\tag{16}$$

$$B_p=\mathbf{H}_p^{-1}\lambda\tag{17}$$

$$K=(\mathbf{H}^T\mathbf{H})^{-1}\mathbf{H}_s.\tag{18}$$

The algorithm proceeds as follows:

1) Hypothesize a set of integers $\mathbf{N_p}=[0,N_2,N_3,N_4]^T$ for the primary measurements. Each of the three "for" loops counts over a range of one of these three integers. If $\overline{N}$ integer values on each side of a nominal integer are hypothesized, then the entire algorithm will be iterated $(2\overline{N}+1)^3$ times.
2) For the hypothesized (primary) integer vector, calculate the corresponding position

$$\begin{aligned}\mathbf{x_p}&=\mathbf{H}_p^{-1}(\tilde{\boldsymbol{\phi}}_p+\mathbf{N_p})\lambda\\&=\mathbf{x}_{\boldsymbol{\phi}}+B_p\mathbf{N_p}.\end{aligned}\tag{19}$$

3) Predict a value for the secondary measurement

$$\hat{\boldsymbol{\phi}}_s=\frac{1}{\lambda}\mathbf{H}_s\mathbf{x_p}.\tag{20}$$

4) Calculate the residual between the predicted and measured secondary phase

$$\hat{\mathbf{res}}_{sp}=(\tilde{\boldsymbol{\phi}}_s-\hat{\boldsymbol{\phi}}_s).\tag{21}$$

This quantity is biased by the secondary integer, which is estimated as

$$\hat{\mathbf{N}}_s=-round(\hat{\mathbf{res}}_{sp}).\tag{22}$$

This choice of $\hat{\mathbf{N}}_s$ does not guarantee a minimal residual for the corrected position due to the possible ill-condi-

tioning of $\mathbf{H}$ [23], but is still used as the alternative is another search over $\hat{\mathbf{N}}_s$.

5) Correct the secondary phase residual for the secondary integer estimate and convert to meters

$$\mathbf{r\hat{e}s}_{sm} = (\mathbf{r\hat{e}s}_{sp} + \hat{\mathbf{N}}_s)\lambda. \tag{23}$$

6) Calculate the correction to $\mathbf{x_p}$ due to the secondary measurements. In a recursive least squares format, under reasonable assumptions [9],

$$\Delta\mathbf{x} = \mathbf{K}\mathbf{r\hat{e}s}_{sm}. \tag{24}$$

7) Calculate the output residual of the position corrected by the secondary measurement

$$\Delta\mathbf{y} = \left(\begin{bmatrix} 0 \\ 0 \\ 0 \\ 0 \\ \mathbf{r\hat{e}s}_{sm} \end{bmatrix} - \mathbf{H}\Delta\mathbf{x} \right). \tag{25}$$

8) Calculate the χ-squared variable q associated with $\Delta\mathbf{y}$. The properly defined χ-squared variable q would account for the covariance matrix of $\Delta\mathbf{y}$ which is straightforward to calculate given $\mathbf{P}_{xs}$. However, due to the required number of on-line calculations the covariance matrix is dropped in favor of the following simpler calculation:

$$q = \frac{\Delta\mathbf{y}^T\Delta\mathbf{y}}{n-4}. \tag{26}$$

9) At this point, three criteria are available to judge the reasonableness of the candidate integer vector $\mathbf{N}_p$:
   a) q should be less that a threshold $\overline{q}$;
   b) $||\mathbf{N}_s||_0 0 \leq \overline{N}$;
   c) $\mathbf{x_p} + \Delta\mathbf{x}$ should be small relative to the aided INS estimate of the position error covariance.

If the calculations corresponding to the integer candidate $\mathbf{N}_p$ satisfy these three conditions, then the vector of hypothesized integers $\hat{\mathbf{N}} = [\mathbf{N}_p, \mathbf{N}_s]$ is saved for future analysis. If any one of the three conditions is violated, then the hypothesized integer vector is discarded.

At the completion of the triple "for" loop, a set of m hypothesized integer vectors $\{\hat{\mathbf{N}}_i, i = 1, \cdots, m\}$ has been constructed. Each vector element of this set has met the test conditions of Step 9) at the given measurement epoch. Depending on the number of satellites available, the noise level, and the satellite geometry, it may take several epochs to reduce the set of hypothesized integers to a single "correct" vector (i.e., $m = 1$). The triple "for" loop describe above is only required for the first epoch, to generate the set of hypothesized integer vectors. On subsequent epochs, each element of the set of hypothesized integer vectors is evaluated by the simpler method of the following section.

2) Reducing the Set of Hypothesized Integer Vectors: After the first epoch [12], the least squares position corresponding to $\hat{\mathbf{N}}_i$ is

$$\hat{\mathbf{x}}_i = \lambda(\mathbf{H}^T\mathbf{H})^{-1}\mathbf{H}^T(\tilde{\phi} + \hat{\mathbf{N}}_i).$$

Therefore, the residual measurement corresponding to $\hat{\mathbf{x}}_i$ is

$$\mathbf{r}_i = (\mathbf{I} - \mathbf{H}(\mathbf{H}^T\mathbf{H})^{-1}\mathbf{H}^T)(\tilde{\phi} + \hat{\mathbf{N}}_i) \tag{27}$$

cycles. The statistics of $\mathbf{r}_i$ can be monitored to remove hypothesized integer candidates, until the number of candidates m is zero or one. If $m = 0$, then the set is empty and the process reinitializes with the triple "for" loop procedure. If $m = 1$, then the procedure has successfully generated a single integer ambiguity vector.

Note that the algorithm is equally valid for the L1, L2, and wide-lane frequencies. In the implementation of this project, the algorithm is used first to determine the wide-lane integers. Then, the increased position accuracy achieved using the wide-lane phase range facilitates the L1 or L2 integer initialization and search.

In the implementation of this project, the above algorithm is processed until only a single vector integer candidate remains (i.e., $m = 1$). The algorithm is then processed again using the identified integer vector as the initial condition until a single vector integer candidate remains. The integer vector is only accepted as correct if the output vector identically confirms (i.e., matches) the initial condition.

Once the correct integers are identified, a similar algorithm is run while monitoring q to determine if cycle slips have occurred. Cycle slip detection is also implemented by comparing and monitoring the code, widelane phase, L1, and L2 ranges.

3) Estimation of N_1^*: The integer search algorithms previously discussed generate the integer vector $\hat{\mathbf{N}} = [0, N_2^* - N_1^*, N_3^* - N_1^*, \cdots, N_m^* - N_1^*]$ and the clock bias estimate $c\delta t_r^* - \lambda N_1^*$. The position correction $\mathbf{x_p} + \Delta\mathbf{x}$ is accurate and could be used to correct the INS. In fact, $(\phi + \hat{\mathbf{N}})\lambda$ could be used as a range estimate in the EKF. All variables estimated would be accurate with the exception of the clock bias. Since the clock bias error is not important to the navigation problem, estimation of N_1^* is not necessary. However, we are interested in estimating N_1^* for two reasons. First, with N_1^* estimated correctly, the L1, L2, widelane, and pseudo-range measurements are all directly comparable. This is useful for residual monitoring and detecting loss of phase lock. Second, the next section describes various modes of INS aiding, the procedure for switching modes was facilitated when N_1 and the clock bias were correct.

In each of modes 2–4 defined in the Section V-B, a DGPS-aided INS system is running while the previously defined integer search process takes place. Therefore, when the integer search succeeds, the DGPS-aided INS system produces a clock bias estimate $t_1 = c\delta t_r$ and the integer search produces a clock bias estimate $t_2 = c\delta t_r - \lambda N_1^*$. The actual estimates of t_1 and t_2 would be corrupted by random errors. The standard deviation of t_1 which results from the complementary filter is less than $\sigma_{MP}/\sqrt{n}$ where σ_{MP} is the standard deviation of the INS aiding signal for the current mode of operation. The standard deviation of t_2 is a small fraction of λ. Therefore, N_1^* can be accurately estimated as $round(t_2 - t_1/\lambda)$. Once N_1^* is determined, it is added to each component of $\hat{\mathbf{N}}$ after scaling by the wavelength to $c\delta t_r$.

IV. Error Covariance Propagation

The discrete time implementation of the EKF requires a discrete-time state propagation matrix and discrete-time equivalent process noise covariance equation. Derivation of appropriate expressions for these two quantities are the subject of this section. The discrete-time state transition is described by

$$\begin{aligned}\mathbf{x}(k+1) &= \boldsymbol{\phi}((k+1)T, kT)\mathbf{x}(k) + \boldsymbol{\omega}_d(k)\\ \mathbf{P}(k+1) &= \boldsymbol{\phi}((k+1)T, kT)\mathbf{P}(k)\boldsymbol{\phi}((k+1)T, kT)^T\\ &\quad + \mathbf{Q}_{\mathrm{d}}(k).\end{aligned}$$

This section specifies the calculation of $\boldsymbol{\phi}((k+1)T, kT)$ and $\mathbf{Q}_{\mathrm{d}}(k)$. For best performance, these variables should be calculated on-line, as they depend on the specific force vector and vehicle to navigation frame transformation.

A. Calculation of State Transition Matrix

The linearized error dynamics for the tangent plane INS are described in (1) and (2). The terms $\mathbf{F}_{vp}$, $\mathbf{F}_{vv}$, and $\mathbf{F}_{\rho p}$ are all small ($< 10^{-6}$) and will be neglected in the calculation of $\boldsymbol{\phi}$. In fact, the term $\mathbf{F}_{\rho\rho}$ is also small for subsonic velocities. By setting the specified terms to zero, expanding the power series of $e^{\mathbf{F}t} = \mathbf{I} + \mathbf{F}t + (1/2)(\mathbf{F}t)^2 \cdots$, and letting $\mathbf{F}_{\rho\rho}$ approach zero, it is straightforward, but tedious, to show that

$$\boldsymbol{\phi}(t_2, t_1) \approx \begin{bmatrix} \mathbf{I} & \mathbf{F}_{pv}T_2 & \frac{1}{2}\mathbf{F}_{pv}\mathbf{F}_{v\rho}T_2^2 & \frac{1}{3}\mathbf{F}_{pv}\mathbf{F}_{v\rho}\mathbf{F}_{\rho g}T_2^3 & \frac{1}{2}\mathbf{F}_{pv}\mathbf{F}_{va}T_2^2 \\ \mathbf{0} & \mathbf{I} & \mathbf{F}_{v\rho}T_2 & \frac{1}{2}\mathbf{F}_{v\rho}\mathbf{F}_{\rho g}T_2^2 & \mathbf{F}_{va}T_2 \\ \mathbf{0} & \mathbf{0} & \mathbf{I} & \mathbf{F}_{\rho g}T_2 & \mathbf{0} \\ \mathbf{0} & \mathbf{0} & \mathbf{0} & \mathbf{I} & \mathbf{0} \\ \mathbf{0} & \mathbf{0} & \mathbf{0} & \mathbf{0} & \mathbf{I} \end{bmatrix} \tag{28}$$

where $T_2 = t_2 - t_1$ is small. By the properties of state transition matrices

$$\boldsymbol{\phi}(t_n, t_1) = \boldsymbol{\phi}(t_n, t_{n-1})\boldsymbol{\phi}(t_{n-1}, t_1) \tag{29}$$

where $\boldsymbol{\phi}(t_n, t_{n-1})$ is defined as in (28) with $\mathbf{F}_{v\rho}$, $\mathbf{F}_{\rho g}$, and $\mathbf{F}_{va}$ defined using the data for $[t_n, t_{n-1})$ and $\boldsymbol{\phi}(t_{n-1}, t_1)$ defined from previous iterations of (29). The iteration of (29) is initialized with $\boldsymbol{\phi}(t_1, t_1) = \mathbf{I}$ and continues for the interval of time propagation to yield $\boldsymbol{\phi}(T, 0)$. At $t = T$, the state error covariance is propagated by

$$\mathbf{P}(T) = \boldsymbol{\phi}(T, 0)\mathbf{P}(0)\boldsymbol{\phi}(T, 0)^T + \mathbf{Q}_{\mathrm{d}}. \tag{30}$$

For the present implementation, $\mathbf{F}_{pv} = \mathbf{I}$, $\mathbf{F}_{\rho g} = \mathbf{R}_{v2t}$, $\mathbf{F}_{va} = \mathbf{R}_{v2t}$, and $\mathbf{F}_{v\rho} = ([f_n, f_e, f_d]\times)$.

B. Calculation of Discrete-Time Process Noise Covariance Matrix

The discrete-time process noise covariance for the $[kT, (k+1)T)$ interval is defined by

$$\mathbf{Q}_{\mathrm{d}}(k) = \int_{kT}^{(k+1)T} \boldsymbol{\phi}((k+1)T, s)\mathbf{Q}(s)\boldsymbol{\phi}((k+1)T, s)^T\, ds$$

where $\mathbf{Q}(t)$ is the continuous time process noise covariance matrix. This integral can be approximated as

$$\mathbf{Q}_{\mathrm{d}}(k) = \sum_{i=1}^{N} \boldsymbol{\phi}(t_{i+1}, t_i)\mathbf{Q}(t_i)\boldsymbol{\phi}(t_{i+1}, t_i)^T\, dT_i$$

where $t_1 = kT$, $t_{N+1} = (k+1)T$, $dT_i = t_{i+1} - t_i$ and $\sum_{i=1}^{N} dT_i = T$. For the present implementation, $dT_i = 0.2$s and

$$\mathbf{Q}(t) = [\mathrm{diag}(\mathbf{Q}_p, \mathbf{Q}_v, \mathbf{Q}_g, \mathbf{Q}_{gd}, \mathbf{Q}_{ad})] \tag{31}$$

where

$$\begin{aligned}\mathbf{Q}_p &= \mathrm{diag}(\sigma_p^2, \sigma_p^2, \sigma_p^2, 1.1 \times 10^{-2})\\ \sigma_p &= 0 \text{ m/s}/\sqrt{\text{Hz}}, \quad \mathbf{Q}_v = \mathrm{diag}(\sigma_v^2, \sigma_v^2, \sigma_v^2, 4.3e-3)\\ \sigma_v &= 1 \times 10^{-2} \text{ m/s}^2/\sqrt{\text{Hz}}, \quad \mathbf{Q}_g = \mathrm{diag}(\sigma_g^2, \sigma_g^2, \sigma_g^2)\\ \sigma_g &= 2.2 \times 10^{-4} \text{ rad/s}/\sqrt{\text{Hz}}, \quad \mathbf{Q}_{gd} = \mathrm{diag}(\sigma_{qd}^2, \sigma_{qd}^2, \sigma_{qd}^2)\\ \sigma_{qd} &= 2.5 \times 10^{-9} \text{ (rad/s/s)}/\sqrt{\text{Hz}}\\ \mathbf{Q}_{ad} &= \mathrm{diag}(\sigma_{ad}^2, \sigma_{ad}^2, \sigma_{ad}^2)\\ \sigma_{ad} &= 1.8 \times 10^{-5} \text{ (m/s/s/s)}/\sqrt{\text{Hz}}.\end{aligned}$$

V. Overall System Design

Given the background of the previous sections, the overall design is straightforward to describe.

A. Hardware Description

The inertial instruments consist of one three axis 2 g accelerometer (manufactured by NeuwGhent Technology, Inc.), and three single-axis fiber optic gyros (Hitachi HGA-D).

The 2 g accelerometer range is large for the lateral and longitudinal accelerations under typical conditions, but required for the vertical acceleration due to the nominal 1g gravitational acceleration. The accelerometer is an inexpensive solid-state device which would be similar to the type of instrument expected in automotive applications.

The gyros have a 10-Hz bandwidth and 60°/s input range. Both characteristics are reasonable for the expected application conditions. A larger bandwidth and input range may be required for emergency maneuvering. The input range must be carefully considered, as resolution and scale factor errors may increase with the input range. The major drawback of the available set of gyros was the designer limited maximum sample rate of 50 Hz via a serial port connection. Although this is five times the sensor bandwidth, it still limits the (proper) INS update rate to 50 Hz. To achieve the desired implementation rate of 100 Hz with minimal delay, each sensed gyro output was assumed constant for two 10.0 ms. sample periods. Even with such sensor deficiencies, the navigation system achieved the desired accuracies and the desired update rate was demonstrated. Overcoming the sensor deficiencies will only improve the demonstrated accuracy. Also, no special coding (e.g., eliminating multiplication of zero matrices) was required to achieve the desired update rates. Additional efforts in algorithm design could substantially increase the INS update and GPS correction rates.

For the experimental results shown later in the report, a compass and tilt meter manufactured by precision navigation were used to initialize the heading, roll, and pitch. The compass was not compensated for local magnetic fields. Even without these sensors, attitude error was rapidly (e.g., one trip around the parking lot) estimated by the EKF. In a commercial application, logic to store and use the last best navigation estimates (at ignition turning off) as the initial conditions for the next run could be considered. Given these two facts, this sensor is not expected to be necessary in commercial applications.

The data acquisition system consists of a 100 MHz IBM 486 compatible with a National Instruments data acquisition board. The GPS hardware consisted of two Ashtech Z-12 receivers. The differential base station to rover serial port connection was a 19 200 baud radio modem.

B. Software Description

The INS operated in the fixed tangent plane system at 100 Hz.[4] The origin was fixed at the location of the base station antenna phase center. The INS was implemented as an interrupt driven background process to ensure the designed update rate.

GPS aiding was implemented by a standard EKF [9], [13] in feedback configuration. The measurement update was implemented at a 1.0 Hz rate with scalar measurement processing. The covariance $\mathbf{R}$ for the each measurement update is dependent on the system mode of operation as defined in the following. Four primary modes of GPS aiding were implemented:

1) *INS only:* This is the default mode of operation. Since INS is implemented as a background process, it continues to run at 100 Hz regardless of mode or the availability of aiding information. When GPS measurements are available, the software automatically switches to Mode 2.
2) *Differential Pseudo-range:* This is the default start-up mode. The primary objectives of this mode are to accurately estimate the navigation state errors and to switch to the widelane phase mode. In this mode the system begins a search and verification process for the widelane integer ambiguities using the algorithm of Section III-D with $\lambda = \lambda_w$. In parallel with the integer ambiguity search, the EKF estimates the navigation state on the basis of the differentially corrected pseudo-range measurements. In this mode, the measurement noise covariance for each measurement is set to $R = 4$ m^2. When the integer search process successfully completes, the software automatically switches to Mode 3.
3) *Differential Widelane Phase:* In this mode, the software attempts to estimate and verify the L1 integer ambiguities using the algorithm of Section III-D with $\lambda = \lambda_1$. In parallel with this integer search, the EKF estimates the navigation state errors using the differentially corrected widelane phase measurements. In this mode, the measurement noise covariance for each measurement is set to $R = 0.1^2$ m^2. When this search process is complete, the software automatically switches to Mode 4. If widelock to at least four satellites is lost, the system automatically reverts to Mode 2.
4) *Differential L1 Phase:* This is the desired system operating mode. To be in this mode, the system will have estimated and verified the L1 integer ambiguities for at least four satellites. While in this mode, the EKF estimates the navigation error state using the differentially corrected L1 phase measurements. The measurement noise covariance for each L1 phase measurement is set to $R = 0.01^2$ m^2.

The INS runs in the background in all four modes. Analysis of the typical time to achieve each mode of operation is presented in Section VI-A.

In modes 3 and 4, the system monitors for loss of lock for each of the "locked" satellites. If lock is lost for a satellite, then the EKF will utilize the differentially corrected pseudo-range for that satellite instead of the corresponding phase measurement. The measurement information is correctly weighted by the EKF by specification of the $\mathbf{R}$ matrix. As long as the system has lock to at least four satellites, the system is usually able to correctly determine the integer ambiguities for "unlocked" satellites by direct estimation ($N^{(i)} = (\mathbf{h}^{(i)}/\lambda)\mathbf{x} - \phi^{(i)}$) instead of search. While in Mode 4, the system will search for L2 integer ambiguities. Once estimated, the L2 phase range is used as a consistency check on the L1 and widelane phase ranges. The consistency check is that the three ranges are equal (within the limits dictated by the various noise factors) and that the integers satisfy $N_w = N_1 - N_2$.

In the differential pseudo-range mode it is possible to also use the differentially corrected Doppler. This would allow on-the-fly (i.e., the vehicle could be moving) integer ambiguity resolution. Due to baud rate limitations, the modem for this implementation could not accommodate Doppler corrections along with the L1 and L2 code and phase pseudorange corrections. Therefore, while in mode 2, we assumed the vehicle was stopped, and synthesized a zero velocity "measurement" with a corresponding value for the sensor uncertainty. This limitation (stationary vehicle) could be eliminated through a faster modem, improved message formatting, or polynomial type correction prediction to decrease the required throughput.

The GPS receiver supplies a pulse aligned with the time of applicability of the GPS measurements. Receipt of this pulse by the INS computer causes the INS state to be saved and used for computation of the predicted GPS observables. The GPS measurements are received over the serial connection 0.4–0.6 s after the pulse (time of applicability). The delay is dependent on the number of satellites. Base corrections also transmitted serially do not arrive until approximately 0.7 seconds after the time of applicability of the GPS measurement. This left 0.3 s to complete the EKF computation of the navigation error state and to correct the navigation system prior to beginning the processing for the next measurement epoch.

An additional improvement which could be added is lever arm compensation. The antenna phase center and accelerometer position do not coincide. For the platform for this project, the separation is approximately 0.6 m in the vertical direction. Therefore, the INS and GPS estimates of position and velocity will differ as the vehicle roll and pitch angles change. For example, a 10° roll or pitch error would result in 10 cm of position error. Lever arm compensation can be achieved through a more involved algorithm for predicting the GPS outputs as a function

[4]Higher rates could be achieved even with the current hardware and software.

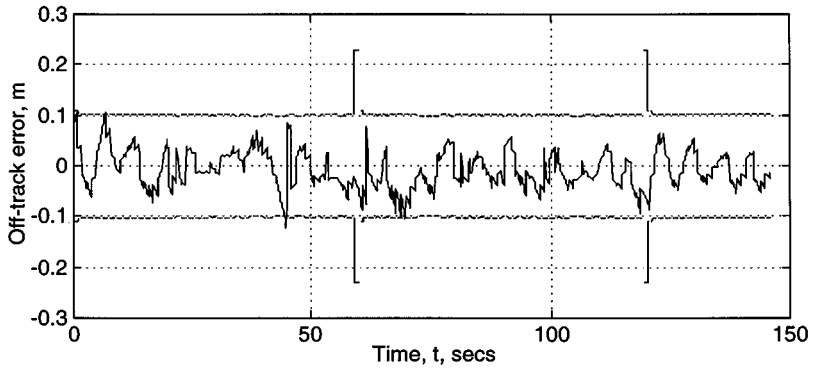

Fig. 2. Table top navigation test. Off-track error versus time. The dashed lines represent the standard deviation of the off-track error calculated from the Kalman filter error covariance matrices.

of the INS state, and an alternative measurement matrix (see [9, Chs. 5 and 7]).

VI. Experimental: Performance Analysis

Section VI-A analyzes the time from initialization to each mode of system operation. The following two sections describe two methods designed to test the positioning accuracy of the DGPS/INS. The primary variable of interest in the analysis, due to the focus on lateral control, was the lateral position accuracy. Analysis of positioning accuracy was difficult due to the lack of independent methods to measure ground truth at the centimeter level. The methodology consists of constraining the navigation system to follow a nominal trajectory. The analysis then focuses on determining the statistics of the estimated position normal to the reference trajectory.

A. Time to Phase Lock Analysis

This section describes results of an experiment designed to analyze the time required for the software to achieve each mode of phase lock described in Section V-B. For each iteration of the experiment, the navigation system software was allowed to run normally until widelock, L1 lock, and L2 lock were all achieved and verified. At this point, the time that each lock status was achieved, the number of satellites, and the estimated position were written to a file. Then a software reset reinitialized the navigation system for the next iteration. The test was performed with a known baseline separation. The estimated position and known baseline were compared to verified correct integer lock during the data analysis phase. The known baseline was not used to aid the integer search.

In the 170 iterations used to generate the following data, there were no instances of incorrect phase lock. There was one eight satellite iteration which did not achieve lock until approximately 900 s. This iteration was excluded from the statistical analysis.

Table I presents the statistics of the total time to achieve each mode of phase lock. Total time is measured from the instant at which the software reset occurs. This time includes a 10-s period during which the system is in Mode 2 while using (14) to initialize the widelane integers prior to initializing the widelane integer search. The indicated lock time is the time at which the integer ambiguities for that phase have been estimated and verified as previously described.

TABLE I
Statistics of the Time to Achieve each Mode of Phase Lock. Time is in Seconds from Initial System Turn On

	Widelock,s	L1 Lock,s	L2 Lock,s
Mean, 7 SV's	35.6	62.0	67.2
STD, 7 SV's	31.5	39.1	40.3
Mean, 8 SV's	40.5	60.1	65.9
STD, 8 SV's	33.9	38.5	38.6

By these statistics, widelane accuracy would on average be available after 36 s. L1 accuracy would be available after 62 s. Note that the algorithm allows the vehicle to be in motion during the search process if differential Doppler corrections are available. Therefore, as long as the average trip to the automated roadway requires in excess of 180 s (i.e., mean time plus three standard deviations), phase lock would be achieved. There is still the potential for performance improvement in the area of integer search algorithms. The algorithm also works well for six satellites, but does not work well for five satellites.

B. Table Top Testing

The experiments of this section involved two steps, both completed while operating in Mode 4. First, the platform was attached to a car and driven around the parking lot for calibration purposes. Second, the platform was transfered to a table and translated repeatedly along two of the table sides. This second step provided a set of trajectories with lateral trajectory accuracy repeatable to one centimeter. Data for two independent repetitions of the experiment are discussed below and in [8].

After placing the navigation platform on the table top, it was cycled between three of the table corners. Motion between the corners maintained a nominally constant heading and nominally kept one platform edge along a table edge. After moving between two points, the platform remained stationary at the destination point for approximately 10 s. During the table top portion of the experiment, INS data was recorded at 10 Hz. Following the experiment, all the stationary data (detected using a threshold of $||v|| < 0.1$ m/s) was separated according to which of the three corner points was closest. The mean and standard deviation of the position data for each corner was tabulated. The calculated corner locations for two runs of the experiment matched with a maximum error of 2.3 cm. The standard devi-

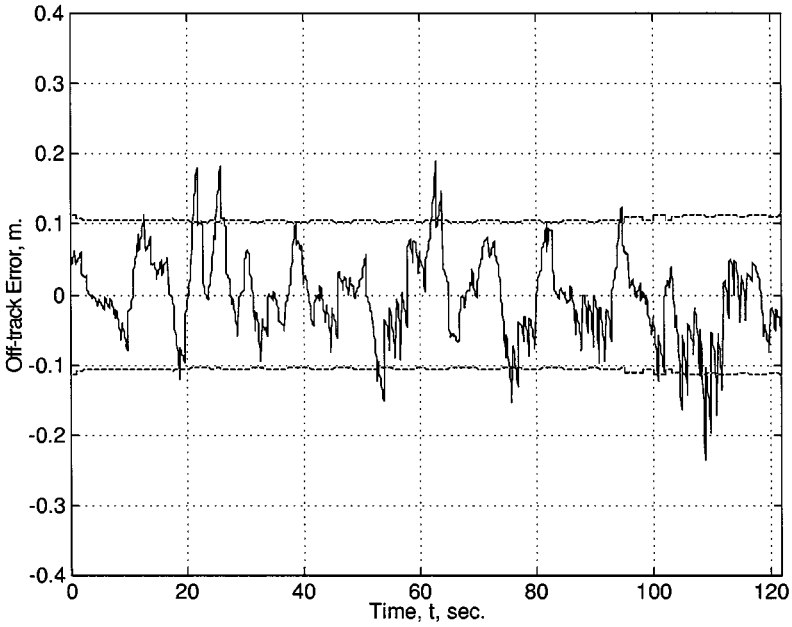

Fig. 3. Amusement park ride L1 Test. Radius error versus time. The dashed lines represent the standard deviation of the off-track error calculated from the Kalman filter error covariance matrices.

ation of the calculated corner locations was 3.8 cm. Note the calculated standard deviations correspond well with the repeatability between the two data sets. Note also that some of the deviation in the calculated corner positions results from the experimenter having to maneuver the platform slowly near each corner to achieve the correct position and alignment.

Fig. 2 presents the off-track error[5] versus time for one experiment. The dashed line on this figure is the navigation system estimate of the off-track error standard deviation, immediately prior to the EKF correction. The off-track error standard deviation was 3.64 cm. This off-track error includes the effects of erroneous motion by the experimenters and multipath. No special multipath precautions were used.

C. Amusement Park Ride Testing

A second set of tests was designed to test the navigation system under significant loading (i.e., accelerations and turn rates). For this experiment, the instrument platform was attached to one of the cars on an amusement park ride. The ride has three intended types of rotational motion. For the experiments described below, two degrees of freedom were fixed so that, nominally, the navigation system follows a circular path inclined to the surface of the earth at about 15°. The ride operator is only able to cycle the ride on or off. When on, the ride accelerates to a rate that would saturate the gyros. When the key is off, the ride automatically applies breaking to slow to a stop. Therefore, for these experiments, the operator had to alternately cycle the ride off and on to keep the ride spinning, but at a reasonable rate. This cycling of the ride is expected to cause mechanical movement and vibration which will cause the actual trajectory to deviate from the nominal circle. In the results that follow, no special precautions were taken either at the base or rover to accommodate multipath effects. Multipath effects should be significant due to the large number of metal surfaces within the amusement park.

The navigation system position accuracy is analyzed by comparing the navigation system position estimates to a curve fit representing the nominal trajectory. Photographs, figures, results of additional experiments, and a detailed description of the experimental analysis can be found in [8].

Three data sets were acquired. Two of the data sets used L1 carrier phase aiding. One of the data sets used widelane carrier phase aiding. Data corresponding to one of the L1 data sets is included herein.

A major source of error in this experiment is mechanical motion, vibration, and flex of the ride which causes the actual path to deviate from its assumed elliptic shape. In addition to the three degrees of rotational freedom, the lever arm, rotational axes, and car are not perfectly rigid or fixed as the unbalanced disk of the ride rotates. Also, the torques necessary to accelerate and deaccelerate the ride as the operator cycles it off and on may cause distortion of the ideal trajectory. Therefore, a significant (but unquantifiable) portion of the "off trajectory error" is caused by the actual trajectory deviating from the assumed ellipse, not by navigation system error.

Fig. 3 displays the off trajectory error versus time for the first L1 experiment. The figure also shows the navigation system estimate of the off-track error standard deviation at a 1 Hz rate, calculated immediately prior to the EKF measurement update. The standard deviation of the experimental off-track error for this L1 experiment was 5.98 cm. This total standard deviation would be explained by 5 cm

[5]See [8] for a detailed description of the method used to calculate off-track error and for plots of other INS variables during this and other experiments.

of ride standard deviation (e.g., mechanical flex) root sum squared with the 2.5 cm of navigation system error standard deviation observed in the table top experiments. Five centimeters of mechanical motion deviation from the least squares trajectory is reasonable. The standard deviation of off-track error for the widelane experiment was 5.50 cm. The widelane GPS position error standard deviation is expected to be $\approx$ 5.6 times that of the L1 phase GPS error standard deviation by (13). The fact that the errors in the two experiments are nearly identical in magnitude indicates that there is a more dominant error source such as the mechanical motion of the ride not exactly following an elliptic path. Therefore, we conclude that the navigation system portion of the error is smaller than the 5 cm of off-track error depicted in the previous figure.

VII. Conclusions and Future Research

This paper presents a differential carrier phase GPS-aided INS methodology and experimental results that achieved the objective a 100 Hz update rate and centimeter level position accuracy. The exact position accuracy achieved is difficult to quantify due to the difficulty of obtaining a second ground truth measurement accurate to at least the centimeter level. The table top evaluation described herein demonstrates an accuracy (i.e., standard deviation) of approximately 2.5 cm, with no special precautions taken to mitigate multipath effects. The amusement park ride experiment demonstrated that the position accuracy was better than 6.0 cm, but beyond this level, the navigation system error could not be discriminated from the mechanical system trajectory error.

The IMU platform for this project was crude by typical INS standards. In this preliminary effort, the authors did not use special test labs or manufacturing facilities for accurate system calibration and alignment. Still, very accurate navigation accuracy was achieved. Better accuracy should be achievable at low cost with a well designed automated manufacturing process which performs an automated set of simple calibration procedures for each instrument, and stores the calibration parameters in onboard nonvolatile memory. Such a process is not unreasonable for the high volume production that could be expected in the automotive industry.

In conclusion, carrier phase DGPS-aided INS approaches provide an accurate, high rate, and reliable navigation solution. With the cost of GPS hardware now below $100 and the cost of INS sensors also decreasing, carrier phase DGPS-aided INS approaches such as that described herein may soon become available for widespread automotive, aircraft, farming, dredging, satellite, and mining applications.

Acknowledgment

Prepared in cooperation with the State of California, Business, Transportation and Housing Agency, Department of Transportation, and Partners for Advance Transit and Highways (PATH). The project was a collaboration between the authors and R. Galijan and J. Sinko from SRI International. The authors gratefully acknowledge the cooperation of Castle Amusement Park and their employees. The contents of this paper reflect the views of the authors who are responsible for the facts and accuracy of the data presented herein. The contents do not necessarily reflect the official views or policies of the State of California. This report does not constitute a standard, specification, or regulation.

References

[1] H. Blomenhofer and G. Hein *et al.*, "Development of a real-time DGPS system in the centimeter range," in *IEEE PLANS*, Las Vegas, NV, 1994, pp. 532–539.
[2] K. R. Britting, *Inertial Navigation Systems Analysis*. New York: Wiley-Interscience, 1971.
[3] R. G. Brown, "Integrated navigation systems and Kalman filtering: A perspective," *Navigation: J. Inst. Nav.*, vol. 19, no. 1, pp. 355–362, 1972–1973.
[4] E. Cannon, "High-accuracy GPS semikinematic positioning: Modeling and results," *Navigation: J. Inst. Nav.*, vol. 37, no. 1, pp. 53–64, Summer 1990.
[5] C. E. Cohen and J. D. Powell *et al.*, "Autolanding a 737 using GPS integrity beacons," *Navigation*, vol. 42, no. 3, Fall 1995.
[6] J. L. Farrell, *Integrated Aircraft Navigation*. New York: Academic, 1976.
[7] J. A. Farrell and T. Givargis, "Differential GPS reference station algorithm: Design and analysis," *IEEE Trans. Contr. Syst. Technol.*, vol. 8, pp. 519–531, May 2000.
[8] J. A. Farrell, M. J. Barth , H. Blomenhofer, and G. Hein *et al.*, "GPS/INS Based Lateral and Longitudinal Control Demonstration: Final Rep., California PATH MOU 292, UCB-ITS-PRR-98-28,", Sept. 1997.
[9] ——, *The Global Positioning System and Inertial Navigation*. New York: McGraw-Hill, 1998.
[10] J. A. Farrell and M. Djodat *et al.*, "Latency compensation for differential GPS," *Navigation: J. Inst. Nav.*, vol. 44, no. 1, pp. 99–107, Spring 1997.
[11] R. Fenton and R. Mayhan, "Automated highway studies at the Ohio State University—An overview," *IEEE Trans. Veh. Technol.*, vol. 40, pp. 100–113, 1991.
[12] R. Galijan, private communication, Jan. 1997.
[13] A. Gelb, *Appl. Opt. Est.*. Cambridge, MA: MIT Press, 1974.
[14] J. Guldner and H.-S. Tan *et al.*, "Analysis of automatic steering control for highway vehicles with look-down lateral reference systems," *Veh. Syst. Dynamics*, vol. 26, pp. 243–269, 1996.
[15] R. Hatch, Instantaneous ambiguity resolutio, in Symp. 107, Kinematic Systems in Geodesy, Surveying and Remote Sensing, Springer Verlag, New York, pp. 299–308, Sept. 1990.
[16] P. Hwang, "Kinematic GPS for differential postioning: Resolving integer ambiguities on the fly," *Navigation: J. Inst. Nav.*, vol. 38, no. 1, Spring 1991.
[17] W.-W. Kao, "Integration of GPS and dead-reckoning navigation systems," in *Proc. Veh. Nav. Inform. Syst. Conf.*, 1991, SAE, pp. 635–643.
[18] C. Kee and B. Parkinson, "Wide area differential GPS as a future navigation system in the US," in *IEEE PLANS*, Las Vegas, NV, 1994, pp. 788–795.
[19] B. Parkinson and P. Axelrad, Global Positioning System: Theory and Applications, vol. II, 1996.
[20] S. Shladover *et al.*, "Automatic vehicle control developments in the PATH program," *IEEE Trans. Veh. Technol.*, vol. 40, pp. 114–130, 1991.
[21] J. W. Spalding and L. A. Luft, Differential GPS integrity monitor, in IEEE PLANS, Las Vegas, NV, USA, pp. 225–232, 1994.
[22] H.-S. Tan, R. Rajamani, and W.-B. Zhang, "Demonstration of an automated highway platoon system," in *Amer. Cont. Conf.*, Philadelphia, PA, 1998, pp. 1823–1827.
[23] P. Teunissen, "A new method for fast carrier phase ambiguity estimation," in *IEEE PLANS*, 1994, pp. 562–573.

Jay A. Farrell (M'85–SM'98) received the B.S. degrees in physics and electrical engineering from Iowa State University, Ames, in 1986, and M.S. and Ph.D. degrees in electrical engineering from the University of Notre Dame, Notre Dame, IN, in 1988 and 1989, respectively.

He joined the technical staff at The Charles Stark Draper Laboratory, Cambridge, MA, in 1989. While at the Draper Lab he was principal investigator on several projects in the areas of intelligent and learning control systems for autonomous vehicles. He joined the faculty of the College of Engineering at the University of California, Riverside in January 1994. He is currently an Associate Professor in and Chair of the Electrical Engineering Department. His current research interests are: identification and on-line control for nonlinear systems, integrated GPS INS navigation, and artificial intelligence techniques for autonomous dynamic systems. He is author of the book "The Global Positioning System and Inertial Navigation" (New York: McGraw-Hill, 1998) and over 60 additional technical publications.

Dr. Farrell received the Engineering Vice President's Best Technical Publication Award in 1990, and Recognition Awards for Outstanding Performance and Achievement in 1991 and 1993. While at Iowa State he received academic excellence scholarships from the Honeywell Foundation and NCR Corporation. While at Notre Dame, he received a Fellowship from the Notre Dame Center for Applied Mathematics. He is a member of the Pi Mu Epsilon, Eta Kappa Nu, Phi Kappa Phi, and Phi Beta Kappa honorary societies.

Tony D. Givargis received the B.S. degree in computer science in 1997 from University of California, Riverside, and is currently working toward the Ph.D. degree at the same school.

His areas of research are developing reusable Intellectual Property cores, system-on-chip design and optimizing on-chip bus structures for reduced power. In addition his research interests include hardware/software system design, embedded systems, and microcontroller-based control systems.

As an undergrad honor student, Mr. Givargis received the Betty P. Ribal mathematics scholarship in 1995, and the International Council on Systems Engineering Scholarship in 1997. He has also received the outstanding academic program excellence and the student commencement awards from Marlan and Rosemary Bourns College of Engineering in 1997. As a first-year graduate student, he received a MICRO fellowship . In 1998, he received the 35th Design Automation Conference Graduate Scholarship.

Matthew J. Barth (M'90) received the B.S. degree in electrical engineering/computer science from the University of Colorado, Boulder, in 1984. He received the M.S. and Ph.D. degrees in electrical and computer engineering from the University of California, Santa Barbara, in 1986 and 1989 respectively.

From 1986 to 1987 he conducted research at the University of Tokyo as a visiting research student in robotics. From 1989 to 1991 he was a Visiting Researcher at Osaka University, Japan, conducting research in robot perception and navigation. He is currently an Associate Professor in the Department of Electrical Engineering at the University of California, Riverside. His research interests include intelligent transportation systems, transportation/emissions modeling, vehicle activity analysis, electric vehicle technology, robotics, and advanced sensing and control.